Analog Integr Circ Sig Process (2016) 87:35–47
DOI 10.1007/s10470-016-0724-2

Joint-digital-predistortion for wireless transmitter's I/Q imbalance and PA nonlinearities using an asymmetrical complexity-reduced Volterra series model

Yue Li[1] · Chak-Fong Cheang[1] · Pui-In Mak[1] · Rui P. Martins[1,2]

Received: 12 November 2015 / Accepted: 14 March 2016 / Published online: 19 March 2016

Abstract I/Q imbalance and nonlinearities of power amplifier (PA) are the main impairments of wireless transmitters degrading the spectral purity and error vector magnitude (EVM). In order to jointly migrate them, an asymmetrical complexity-reduced Volterra series model is proposed, namely joint-digital predistortion (joint-DPD). Our joint-DPD is inspired by the interaction between such two impairments, providing high degree of dynamic nonlinearities with large memory depths. Also, by understanding the structure of joint-DPD for OFDM signals, lower computational complexity can be achieved by pruning the redundant terms with an asymmetrical structure. The corresponding analysis offers the theoretical basis and its related complexity over different Volterra-series-based joint-DPDs. The performances are evaluated under two scenarios. Especially when a 3.4-dB back-off input power is applied, where severe PA nonlinearities are presented with the I/Q imbalance, the measured (left, right) adjacent channel power ratio is improved from (−19.9, −19.6 dBc) to (−37.3, −37.9 dBc), and the EVM is reduced from 22.1 to 3.4 %. For performance comparison, other Volterra-series-based DPDs such as memory polynomial, dynamic deviation reduction and generalized memory polynomial, are also extended to joint-DPD.

Keywords Computational complexity · Digital predistortion (DPD) · I/Q imbalance · Power amplifier (PA) · OFDM · Volterra series

1 Introduction

Orthogonal frequency-division multiplexing (OFDM) is a multicarrier modulation technique used for boosting the system throughput in modern wireless systems [1]. Yet, OFDM is sensitive to a wide variety of non-idealities in the transmitter front-end [2]. As modeled in Fig. 1(a) for a direct-conversion transmitter, the in-phase and quadrature (I/Q) imbalance [3] and the power amplifier's (PA) nonlinearities with memory [4] are the two main impairments limiting the performance. Generally, I/Q imbalance brings about inter-carrier interference (ICI), which puts a significant threat to the OFDM symbol accuracy. For the PA operation, smaller power back-off certainly benefits the power efficiency, but also induces more severe nonlinearities and memory effects due to the high peak-to-average-power ratio (PAPR) property of the OFDM signal [2, 5, 6]. Thus, exploring an effective digital calibration technique that can jointly address these two impairments becomes attractive.

In the aspects of flexibility and capability, the adaptive digital predistortion (DPD) dominates the contents of PA distortion compensation [7–13]. PA model and predistorters can be based on Wiener [7], separable function [8], or the pruned Volterra series [9–14], which is capable to account the frequency-dependent impairments. Memory polynomial (MP) DPD [11] is a low-complexity model with no cross dynamics, representing severe memory effects being involved. Dynamic deviation reduction (DDR) DPD [12] restricts the expression in terms of

R. P. Martins—On leave from Instituto Superior Técnico, Universidade de Lisboa, Portugal.

✉ Pui-In Mak
pimak@umac.mo

[1] State-Key Laboratory of Analog and Mixed-Signal VLSI and Faculty of Science and Technology - Department of ECE, University of Macau, Macao, China

[2] Instituto Superior Técnico, Universidade de Lisboa, Lisbon, Portugal

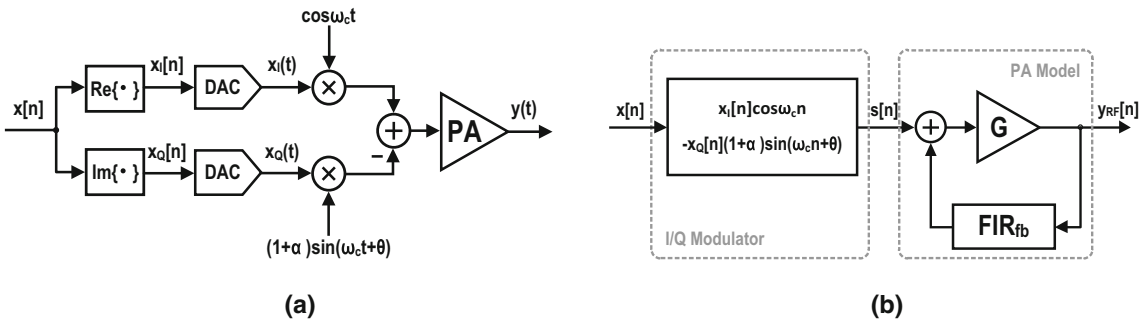

Fig. 1 **a** Direct-conversion transmitter with I/Q imbalance and a nonlinear PA. **b** Simplified discrete-time-domain equivalence with a feedback PA model

dynamic order. Thus, the complexity of the model goes up significantly when the order of dynamics is expanded. The generalized memory polynomial (GMP) DPD [13] provides large diversity of cross dynamic terms by deploying additional leading/lagging memory depth. Yet, this also produces extra complexity on the model construction. The complexity-reduced Volterra series (CRV) DPD [14] is derived from the feedback topology, providing high nonlinear orders and large memory depth in a complexity efficient way. The complexity-accuracy of PA-DPD is compared in [15]. Besides, Volterra-series DPD has also shown an excellent compensation performance for frequency-dependent I/Q imbalance [16].

Joint-DPD can be constructed by the polynomial based predistorter as described in [17–20]. Memoryless polynomial is deployed in [17], thus the performance will be degraded significantly when large dynamic cross-terms appear. Mildly inter-channel nonlinear dynamic effects and I/Q imbalances are compensated in cascade with MP predistorter. In [18–20], the structure takes frequency-dependent impairments into account by extending the MP predistorter. Yet, due to the scarcity of cross dynamics, MP performs weakly on modeling and compensating severe PA nonlinearities and memory effects [14, 20, 21]. In addition, there is no evaluation on symbol accuracy in Refs. [18] and [19], such as normalized mean square error (NMSE) and error vector magnitude (EVM). This renders the results less convincing, because in OFDM systems the I/Q imbalance cannot be observed in spectra [18].

This paper focuses on the basis construction and dispersal analysis on different pruning techniques for memory DPDs including MP, 1st-order DDR (DDR1), 2nd-order DDR (DDR2), GMP and CRV, in terms of static nonlinear order, memory depth dynamic order and the number of cross terms. Also, the advanced asymmetrical complexity-reduced Volterra series (ACRV) model is proposed to develop a joint-DPD to compensate both the frequency-dependent I/Q imbalance and PA nonlinearities. A closed-form expression is derived to provide flexibility for the different levels of impairments such as I/Q imbalance, higher order nonlinearity and larger memory depth. The asymmetrical joint-DPD structure is proposed based on the analysis of the pruning method for OFDM applications. Meanwhile, the analysis also provides a theoretical proof why the joint-DPD can tackle I/Q imbalance by adding only conjugate terms and can be generalized to different DPDs, which were not explained in Refs. [17, 18]. The complexity-accuracy of the joint-DPD is comprehensively studied via the number of floating point operations (FLOPs), evidencing the efficiency of the asymmetrical structure. Finally, the following techniques: MP [11], GMP [13] with only odd-order nonlinearities: DDR1 and DDR2 [12] are also extended to joint-DPD for performance comparison with the proposed solution.

This paper is organized as follows. In Sect. 2, basis construction and its dispersal properties is introduced. After extending the CRV to a joint model in Sect. 3, the proposed asymmetrical joint-DPD is introduced and its computational complexity is analyzed. In Sect. 4, measurement setup and performance metrics are described, followed by the experimental results of two scenarios. Several Volterra-series-based methods are also extended to joint-DPD for comparison. Finally, the conclusion is drawn in Sect. 5.

2 ACRV model and predistorter

In [18], joint-model and predistorter can be achieved by adding the conjugated part of PA model directly into the original one, which replace the input x[n] to its conjugate x*[n]. Here, the ACRV model is introduced to ease the tradeoff between complexity and efficiency. Its related computational complexity is further analyzed using FLOPs.

2.1 Joint ACRV model

Based on the feedback topology [22, 23] given in Fig. 1(b), a PA model of CRV is derived [14]. Its closed-form RF equivalent expression is written as

$$y_{RF}[n] = G(s[n]) + \sum_{i=0}^{P-1}\sum_{j=1}^{M}\sum_{k=1}^{P} a_{ijk}s^i[n]s^k[n-j] \quad (1)$$

where s[n] and y[n] are the discrete-time RF signal of the PA input and output signals, respectively. a_{ijk} is the Volterra kernel of the dynamic cross terms. M is the memory depth. P is the nonlinear order of a static nonlinear function of G, which is defined as

$$G(s[n]) = \sum_{i=1}^{P} h_i s^i[n] \quad (2)$$

where h_i can be considered as the static kernels with ith-order static nonlinearity. Since the frequency-dependent, nonlinear I/Q imbalance can also be modeled by the nonlinear memory effect after the joint-model, only frequency-independent I/Q imbalance of the modulator is thus involved in the model as shown in Fig. 1(b). The PA input $s[n]$ can be expressed as [24]

$$s[n] = x_I[n]\cos\omega_c n - x_Q[n](1+\alpha)\sin(\omega_c n + \theta) \quad (3)$$

where $x_I[n]$ and $x_Q[n]$ are the real and imaginary parts of the transmitter input x[n], respectively. α and θ represent the amplitude and phase imbalances, respectively. With the expression $x_I[n] = \frac{1}{2}(x[n] + x^*[n])$ and $x_Q[n] = \frac{1}{2j}(x[n] - x^*[n])$, s[n] can be further derived to

$$s[n] = Ax[n]e^{j\omega_c n} + Bx^*[n]e^{-j\omega_c n} + Cx[n]e^{-j\omega_c n} + Dx^*[n]e^{j\omega_c n} \quad (4)$$

where the four complex coefficients are replaced by

$$A = \frac{1}{4}\left[1 + (1+\alpha)e^{j\theta}\right];\ B = \frac{1}{4}\left[1 + (1+\alpha)e^{-j\theta}\right];\ C = \frac{1}{4}\left[1 - (1+\alpha)e^{-j\theta}\right];\ D = \frac{1}{4}\left[1 - (1+\alpha)e^{j\theta}\right]$$

The coefficient C and D are much smaller than A and B since the I/Q imbalance is commonly within a range of $\alpha \le 5\,\%$ and $\theta \le 5^\circ$ [16, 18]. Considering no I/Q imbalance, i.e., $\alpha = 0$ and $\theta = 0$ (7) will become $2s[n] = x[n]e^{j\omega_c n} + x^*[n]e^{-j\omega_c n}$ which is the ideal transformation from RF to baseband expression.

Since the signal and mirror interferences generated by the I/Q imbalance will be fed into the PA, the joint baseband expression of CRV PA model and I/Q imbalance can be derived by substituting (7) into (4). To clearly illustrate the derivation, the term $s^i[n]$ with $i = 3$ in $G(s[n])$ is considered first. It leads to

$$s^3[n] = (Ax[n]e^{j\omega_c n} + Bx^*[n]e^{-j\omega_c n} + Cx[n]e^{-j\omega_c n} + Dx^*[n]e^{j\omega_c n})^3 \quad (5)$$

By extending (8), totally 20 terms will be resulted. However, components far from the carrier frequency can be eliminated from the PA output. Thus, only the terms related to $e^{j\omega_c n}$ ill remain in the final expression. The baseband equivalent $s^3_{BB}[n]$ of $s^3[n]$ becomes

$$s^3_{BB}[n] = (AAB + ADC)x[n]|x[n]|^2 + (ADB + DDC)x^*[n]|x[n]|^2 + AAC(x[n])^3 + DDB(x^*[n])^3 \quad (6)$$

Considering two symmetrical tones located at $-f_\Delta$ and f_Δ are applied as the input signal as shown in Fig. 2, the output generated corresponding to the four terms overlap at $-3f_\Delta$, $-f_\Delta$, f_Δ and $3f_\Delta$ in the frequency domain. Thus, if an OFDM signal with $2N$ subcarriers and f_Δ subcarrier spacing experiences I/Q imbalance and Pth odd-order nonlinearities, the distorted output generated by each nonlinear term will overlap in the spectral interval $(-NPf_\Delta, NPf_\Delta)$ with f_Δ spacing. It indicates that the terms representing the joint effect of I/Q imbalance and PA nonlinearities have a similar spectral behavior for OFDM applications. Considering the influence of each coefficient in (9), the magnitude between each coefficient has been simulated. The maximum value for the third and fourth terms of (9) are simulated as,

$$\frac{|AAC| + |DDB|}{|AAB + ADC| + |ADB + DDC| + |AAC| + |DDB|} < 5\,\% \quad (7)$$

Also, the interaction of I/Q imbalance and PA nonlinearities can thus be represented by $x[n]|x[n]|^2$ and its conjugate $x^*[n]|x[n]|^2$ which are sufficed to carry the necessary information. The expression complexity is nearly halved by this elimination. Another important issue for choosing $x^*[n]|x[n]|^2$ rather than $(x[n])^3$ is its relaxed complexity as conjugating $x[n]|x[n]|^2$ consumes negligible computational

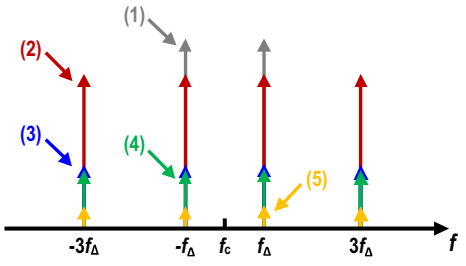

Fig. 2 Spectral behavior of (*1*) original signal $x[n]e^{j\omega_c n}$ (*2*) $(AAB + ADC)$ (*3*) $(ADB + DDC)x^*[n]|x[n]|^2e^{j\omega_c n}$, (*4*) $AAC(x[n])^3$ and (*5*) $DDB(x^{*[n]})^3e^{j\omega c^n}$

effort in the basis construction [20]. Thus, third and fourth terms in (9) are eliminated.

Extending this result to higher order nonlinearities and dynamics in (4), redundant terms can be further abandoned. Besides, in the image part, $x^*[n]|x[n]|^2$ describes the inter-modulation between the image tones, which has much smaller magnitudes in the coefficients than the signal part $x[n]|x[n]|^2$. The image harmonics with magnitudes close to the noise floor can be further eliminated. Thus, the parameters of image parts are separated with the signal parts with different nonlinear order (P_i) and memory depth (M_i) in order to relax the complexity. This kind of complexity relaxing configuration on image related tones is defined as the *asymmetrical joint-DPD structure*. The baseband equivalent expression of joint I/Q modulator and RF PA model based on (4) can be derived as

$$\begin{aligned} y_{ACRV}[n] = & \sum_{\substack{p=1 \\ p\,odd}}^{P} h_p x[n]|x[n]|^{p-1} + \sum_{\substack{p=1 \\ p\,odd}}^{P_i} h_p^i x^*[n]|x[n]|^{p-1} \\ & + \sum_{\substack{p=1 \\ p\,odd}}^{P-2} \sum_{\substack{k=2 \\ k\,even}}^{P-1} \sum_{m=1}^{M} a_{p,k,m} x[n]|x[n]|^{p-1}|x[n-m]|^k \\ & + \sum_{\substack{p=0 \\ p\,even}}^{P-1} \sum_{\substack{k=1 \\ k\,odd}}^{P} \sum_{m=1}^{M} b_{p,k,m} x[n-m]|x[n]|^{p}|x[n-m]|^{k-1} \\ & + \sum_{\substack{p=1 \\ p\,odd}}^{P_i-2} \sum_{\substack{k=2 \\ k\,even}}^{P_i-1} \sum_{m=1}^{M_i} a_{p,k,m}^i x^*[n]|x[n]|^{p-1}|x[n-m]|^k \\ & + \sum_{\substack{p=0 \\ p\,even}}^{P_i-1} \sum_{\substack{k=1 \\ k\,odd}}^{P_i} \sum_{m=1}^{M_i} b_{p,k,m}^i x^*[n-m]|x[n]|^{p}|x[n-m]|^{k-1} \end{aligned} \tag{8}$$

where P_i and M_i are the nonlinear order and memory depth of the image part, respectively. $a_{p,k,m}$ and $b_{p,k,m}$ re the Volterra kernels for the signal part, whereas $h_p^i a_{p,k,m}^i$ and $b_{p,k,m}^i$ are for the image part. Hence, the image part can have different (mostly smaller) parameters than the signal part to relax the complexity, implying an asymmetrical structure. To explore this, a comprehensive parameter-pruning process is provided in Sect. 3, focusing on the structural complexity-accuracy evaluation by using the best performance metrics (ACPR and EVM) versus FLOPs.

The new formulation (11) can be learned as an ACRV behavioral model for joint-DPD of I/Q imbalance and PA nonlinearity. It inherits the benefits of CRV [14] providing high degree of dynamic nonlinearities with large memory depths. Note that the asymmetrical expansion can also be applied to other Volterra-series-based PA models in [11–13] as asymmetrical MP (AMP), asymmetrical GMP (AGMP) and ADDR1 and ADDR2 likewise.

2.2 Joint-DPD

Based on the pth-order inverse theory [25], it has been concluded in [26] that a Volterra-series-based predistorter has the same structure with the corresponding model. Thus, the predistorter H^{-1} in Fig. 3 can be directly written as

$$\begin{aligned} x[n] = \mathrm{H}^{-1}(u[n]) = & \sum_{\substack{p=1 \\ p\,odd}}^{P} h_p u[n]|u[n]|^{p-1} \\ & + \sum_{\substack{p=1 \\ p\,odd}}^{P_i} h_p^i u^*[n]|u[n]|^{p-1} \\ & + \sum_{\substack{p=1 \\ p\,odd}}^{P-2} \sum_{\substack{k=2 \\ k\,even}}^{P-1} \sum_{m=1}^{M} a_{p,k,m} u[n]|u[n]|^{p-1}|u[n-m]|^k \\ & + \sum_{\substack{p=0 \\ p\,even}}^{P-1} \sum_{\substack{k=1 \\ k\,odd}}^{P} \sum_{m=1}^{M} b_{p,k,m} u[n-m]|u[n]|^{p}|u[n-m]|^{k-1} \\ & + \sum_{\substack{p=1 \\ p\,odd}}^{P_i-2} \sum_{\substack{k=2 \\ k\,even}}^{P_i-1} \sum_{m=1}^{M_i} a_{p,k,m}^i u^*[n]|u[n]|^{p-1}|u[n-m]|^k \\ & + \sum_{\substack{p=0 \\ p\,even}}^{P_i-1} \sum_{\substack{k=1 \\ k\,odd}}^{P_i} \sum_{m=1}^{M_i} b_{p,k,m}^i u^*[n-m]|u[n]|^{p}|u[n-m]|^{k-1} \end{aligned} \tag{9}$$

where $u[n]$ is the original input. It is proved [25] that the pth-order pre-inverse $x[n] = \mathrm{H}^{-1}(u[n])$ is identical to the pth-order post-inverse. H^{-1} can be extracted directly from $u[n]$ and $y[n]$, as $u[n] = \mathrm{H}^{-1}(y[n])$ Considering the multi-linear properties of Volterra series, least square (LS)

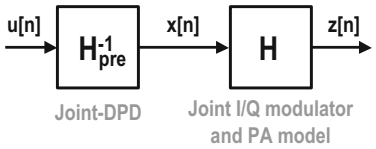

Fig. 3 Proposed joint-DPD for calibration of I/Q imbalance and PA nonlinearity together

algorithm is deployed for extracting the parameters of the joint-DPD. A parameter vector φ an be constructed with containing $h_p a_{p,k,m} b_{p,k,m} h_p^i a_{p,k,m}^i$ and $b_{p,k,m}^i$ in (12). A signal matrix $\mathbf{Y}$ is then constructed by including all of the product terms $y[n]|y[n]|^{p-1}y[n]|y[n]|^{p-1}|y[n-m]|^k y[n-m]|y[n]|^p|y[n-m]|^{k-1}y^*[n]|y[n]|^{p-1}y^*[n]|y[n]|^{p-1}|y[n-m]|^k$ and $y^*[n-m]|y[n]|^p|y[n-m]|^{k-1}$ for $n=M+1,\ldots,L$ where L is the total length of the captured data. The expected output vector is $\mathbf{x}=[x[M+1],\ldots,x[L]]^T$ where $[\cdot]^T$ Represents the transpose operation, and the modeling error vector $\mathbf{e}=[e[M+1],\ldots,e[L]]^T$ s defined, where $e[n]=x[n]-y[n]$. Thus, the Volterra series model can be generally written as

$$\mathbf{x} = \mathbf{Y}\boldsymbol{\varphi} + \mathbf{e} \tag{10}$$

A solution for φ an be estimated as $\hat{\varphi}$ minimizing the cost function $J(\varphi) = \mathbf{e}^H\mathbf{e}$ where $[\cdot]^H$ represents Hermitian transpose. The pre-inverse joint-DPD parameters can be extracted by LS solution, which is

$$\hat{\boldsymbol{\varphi}} = \left(\mathbf{Y}^H\mathbf{Y}\right)^{-1}\mathbf{Y}^H\mathbf{x} \tag{11}$$

2.3 Complexity

A comprehensive methodology for analyzing the complexity-accuracy tradeoff in PA behavioral modeling has been reported in [21]. It can also be extended to the performance of the joint-DPD. For the proposed ACRV model, the complexity for constructing basis functions can be calculated as

$$C_{\mathrm{ACRV,basis}}(P,M,P_i,M_i) = 3 + (\max(P,P_i)-1) + 2\max(PM,P_iM_i) \tag{12}$$

where 3 is the square construction (Table 1 in [21]). $(\max(P,P_i)-1)$ is the FLOPs consumed for the static nonlinear construction in (12), by choosing the maximum complexity between the signal and its image. Besides, $2\max(PM,P_iM_i)$ is the FLOPs consumed for the dynamic part that describes the complexity of delay and complex-real multiplications of the static terms. The total number of coefficients f_{ACRV} in each basis kernel for ACRV is calculated as

$$f_{\mathrm{ACRV}}(P,M,P_i,M_i) = \frac{P+1}{2} + \frac{M}{2}\left(P^2+1\right) + \frac{P_i+1}{2} + \frac{M_i}{2}\left(P_i^2+1\right) \tag{13}$$

where the first two terms are the number of coefficients in the signal, and the last two terms are for its image. Complexities for constructing basis and the number of coefficients of other four competitive structures are extended to joint predistorters, which are included in the Appendix. The overall complexity of each DPD can be calculated accordingly.

Table 1 Range of parameters for different joint-DPD

Model	Nonlinearity order (P, P_i, odd only)	Memory depth (M, M_i)	Leading/lagging depth (K, K_i, for GMP only)
ACRV	[3:2:11]	[1:4]	–
AMP	[3:2:21]	[1:10]	–
ADDR1	[3:2:15]	[1:5]	–
ADDR2	[5:2:15]	[1:3]	–
AGMP	[3:2:15]	[1:4]	[1:4]

3 Experimental results

In this section, the proposed joint-DPD and others are characterized with a wide range of parameters as shown in Table 1 (detailed illustration is given in Sect. 3.2). Qhull algorithm (Qhull 2012. 1, Available: http://www.qhull.org) is deployed to find the best performance line for each type of DPD [21]. The most complexity-efficient parameter settings are chosen to make the forward performance validation, which allows comparing the effectiveness of each DPD.

3.1 Experimental setup

The experimental setup for both DPD extraction and forward performance validation is shown in Fig. 4(a, b). An Agilent E4438C vector signal generator (VSG) is employed to generate a systematic I/Q imbalance to the test signal. The I/Q imbalance is set to 5 % amplitude and 5° phase mismatches, which are severe enough to show the capability of each DPD in terms of I/Q correction [16, 18]. The device-under-test (DUT) is a 1-W commercial MAX2242 PA from Maxim Integrated as shown in Fig. 4(b). It operates at 2.4–2.5 GHz, with a power gain of 28.5 dB and output power of +22.5 dBm. Note that the output power is comparatively small with the PA used in the base station. However, if the input power of the DUT is bursted to relatively small back-off power (Scenario 2), severe nonlinearities and memory effect are generated. An Agilent DSO91304A digital storage oscilloscope (DSO) synchronized by a 10-MHz trigger signal with the VSG, is utilized to capture the DUT's input and output for further signal processing in MATLAB. A 20-dB attenuator (RADIALL R413820000) is employed to lower the power of PA output to meet the DSO's requirement with an 8-dB increment of noise floor. The test data is a 20-MHz

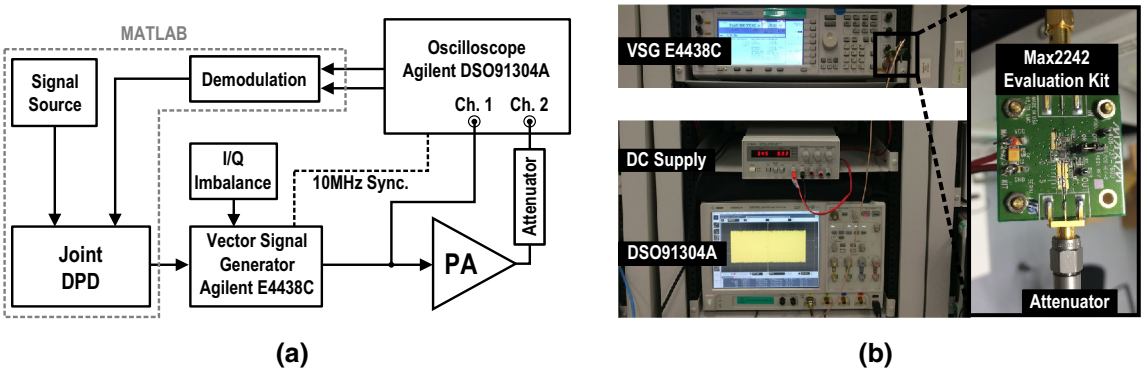

Fig. 4 Measurement setup for both joint-DPD identification and forward performance validation in **a** block diagram and **b** photo of testbench

bandwidth, 64-QAM OFDM signal with 8.03-dB PAPR, 52 active subcarriers out of 64, 312.5-kHz subcarrier spacing and 5× oversampling. This test signal is modulated to a 2.44-GHz carrier, and measured as having an EVM of 1.786 % and ACPR of (−40.1 dBc, −39.8 dBc), and the measured input EVM goes to 5.399 % when above I/Q imbalance is set by the VSG. Different sets of data are captured for extraction and validation separately. Each set contains 16,000 samples with 50 OFDM symbols to ensure that at least 200 parameters can be accurately estimated [26].

The DUT is operated at two power levels: with output power at 8- and 4.4-dB relative back-off from the saturation power. These two scenarios correspond to medium and severe RF nonlinearities and memory effects, suitable for assessing the calibration capability of the proposed joint-DPD.

A wide range of nonlinear orders (odd only) and memory depths for both signal and image parts are explored for each joint-DPD as shown in Table 1. The parameters in Table 1 are determined by considering the extraction capability of the data sets, and the variation of complexity among DPD structures. Since the ACRV has actually $2P$-1 order of nonlinearity, 11th order is set as the limit. Besides, same range of parameters is also explored on CRV for comparison between PA-DPD and joint-DPD. As shown in Table 1, there are 400 different settings explored for ACRV, 10,000 for AMP and totally over 24,000 settings for all the DPDs. It is impractical to forward validate all the parameter settings. Thus, an evaluation of those parameters is performed in computer first. The setting with best performance of each DPD is chosen for the forward performance validation. For the computer process, the kernels of each DPD with different settings are all extracted offline by the measured I/O signals of the transmitter. Then the system output is introduced to the extracted predistorter and the resulted DPD output is compared to the original system input to gain an evaluation of the DPD performance. Qhull algorithm is then employed to find convex hull of the settings of each DPD, providing the best performance line for further analyses. This is marked as the simulated calibration performance.

Besides, for the metrics of the DPD evaluation, EVM is used as the measure of time-domain-signal accuracy, and the adjacent channel error power ratio (ACEPR) [21] and ACPR are used for measuring the spectral accuracy. EVM provides better intuitive sense on symbol accuracy for the test signal in this measurement. ACEPR is considered to be the best measure to identify nonlinear mismatches [5, 21]. Thus, in the DPD extracting stage, ACEPR is used to validate the harmonic reduction performances on each structure. ACPR is used in the forward performance validation, because it is directly related to the standard spectral mask and can be easily captured from the spectrum analyzer (PXA Signal Analyzer Agilent N9030A).

3.2 Scenario 1: output power at 8-dB back-off

As a comparison between PA-DPD and joint-DPD, the simulated calibration performance of ACRV respect to FLOPs is plotted together with CRV in Fig. 5. Although the interaction between nonlinearities and I/Q imbalance can be modeled by PA-DPD, the accuracy of the PA-DPD is strictly limited by the system I/Q imbalance. As I/Q imbalance mainly contribute to the symbol inaccuracy, all impairments can be addressed separately by I/Q compensator and PA-DPD. The EVM is sufficed here for the PA-/Joint-DPD comparison. Also, the simulated performance of ACRV is also presented in Fig. 6 together with other joint-DPDs. All the Joint-DPDs' performance in terms of EVM and ACEPR improvements are limited at FLOPs >500. Thus, the best performance parameters for forward validation are selected within a reasonable range, FLOPs <1000 to acquire the maximum capability of each DPD. For the proposed ACRV, the parameters are selected as $P = 9$, $M = 2$, $P_i = 5$, $M_i = 1$ with totally 869 FLOPs.

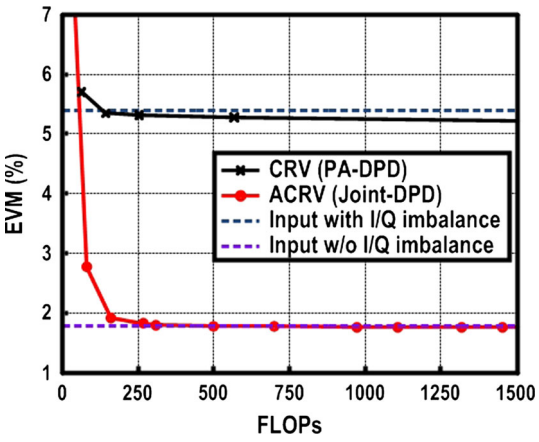

Fig. 5 Scenario 1: Output power at 8-dB back-off from the saturation power. Comparison between CRV and ACRV via EVM versus FLOPs. The reason that the EVM of CRV can go slightly lower than the input with I/Q imbalance is due to the fact that, the PA nonlinearities is not very severe in that scenario, making CRV can compensate a fraction of I/Q interferences that behave similarly with some PA nonlinearities

Jointly pre-compensated signals are generated correspondingly and fed to the system for validation. Constellations of system output with proposed ACRV and with the PA-DPD CRV are shown in Fig. 7(a, b), respectively. It shows that the ACRV has jointly compensated the I/Q imbalance and PA nonlinearities with an improved EVM from 8.7 to 2.7 %, while the CRV is only capable of reducing to 5.926 %. As the interaction between nonlinearities and I/Q imbalance generate the nonlinear memory effect, AM/AM and AM/PM plots have a similar characteristic (but more divergence). In Fig. 8(a, b), the AM/AM and AM/PM plots for the system output without and with ACRV joint-DPD are presented through I/Q imbalance, respectively. All the nonlinearities, memory effects and the phase-shift due to the introduced I/Q imbalance are well compensated. Out-of-band distortions are also significantly suppressed. The (left, right) ACPR of system output is improved from (−29.6 dBc, −28.9 dBc) to (−39.5 dBc, −39.1 dBc). Spectrum of the system output compensated

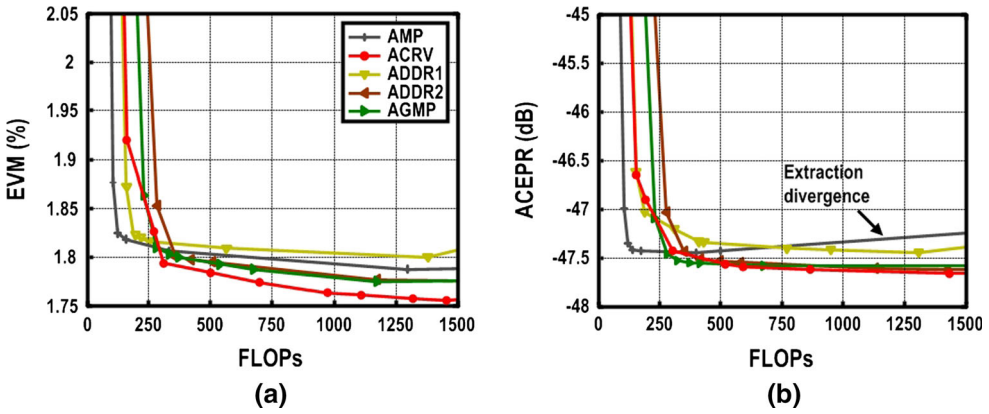

Fig. 6 Scenario 1: ADDR1 and ADDR2 stand for asymmetrical first- and second-order Volterra DDR joint DPDs, respectively. **a** EVM versus FLOPs. **b** ACEPR versus FLOPs. The extraction of MP diverges when the complexity goes high, because the nonlinear orders beyond 17 may count against the out-of-band accuracy. This observation shows ACEPR may be more critical for characterizing joint-DPD than EVM

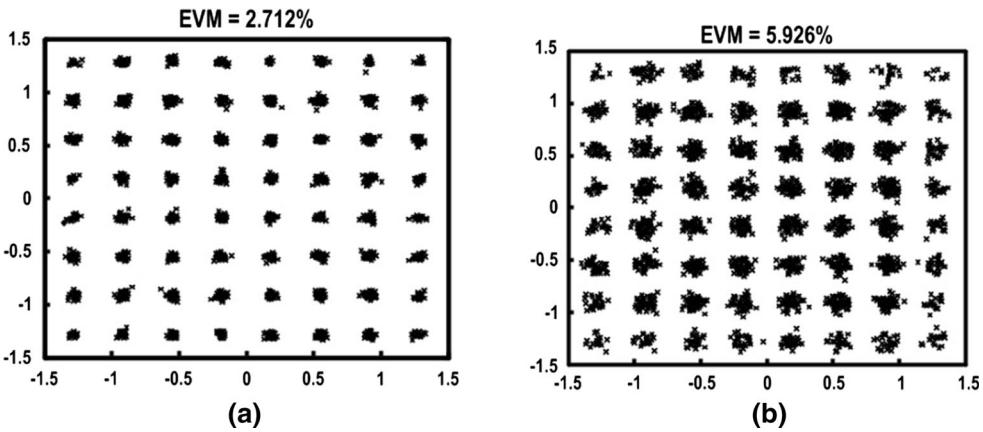

Fig. 7 Scenario 1: Output power at 8-dB back-off from saturation power. Measured constellation diagrams: **a** system output with proposed ACRV joint-DPD, and **b** with CRV PA-DPD

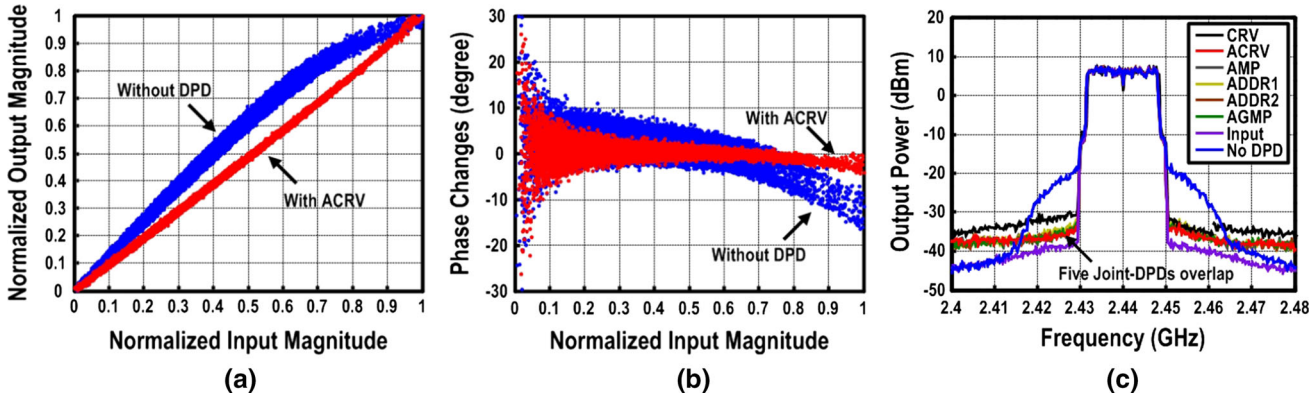

Fig. 8 Scenario 1: Output power at 8-dB back-off from the saturation power. **a** AM/AM and **b** AM/PM plots for the system output without DPD, and with proposed ACRV joint-DPD. **c** Spectra plots of the system input, output without DPD and output with different kinds of joint-DPDs

Table 2 Selected parameters of each DPD for performance validation

Model	Parameters	FLOPs	$\text{ACEPR}_{\text{sim}}$	EVM_{sim}	EVM_{meas}	ACPR_{sim}	$\text{ACPR}_{\text{meas}}$
ACRV	(9,2,5,1)	869	−47.63	1.781	2.712	(−41.52, −41.17)	(−39.5, −39.1)
AMP	(15,2,15,2)	399	−47.44	1.820	2.881	(−41.37, −41.73)	(−39.4, −38.5)
ADDR1	(11,4,11,4)	953	−47.43	1.811	3.033	(−41.24, −40.84)	(−38.9, −38.2)
ADDR2	(11,1,9,1)	585	−47.56	1.795	2.730	(−41.40, −41.09)	(−39.0, −38.3)
AGMP	(15,1,1,15,1,1)	669	−47.58	1.788	2.803	(−41.46, −41.20)	(−39.8, −39.0)

Corresponding simulated and experimental calibrating performance for Scenario 1

by ACRV is plotted together with other competitive DPDs in Fig. 8(c). For all considered DPDs, the key indexes are listed in Table 2. Evidenced by the higher EVM, the performance of the PA-DPD of CRV is limited by the I/Q imbalance, which also cause interferences to the adjacent channels. For AMP, ADDR1, ADDR2 and proposed ACRV, the parameters are presented in the manner of (P, M, P_i, M_i) and (P, M) for the CRV. For AGMP with only nonlinear orders and causal terms being involved, its parameters are presented as $(P,M,K,P_{\text{i}},M_{\text{i}},K_{\text{i}})$. All joint-DPDs have similar experimental performance on EVM and ACPR reduction just as the simulation shows. Comparing to basis construction of different DPDs, ADDR1 achieves similar EVM and ACPR performance in simulations with largest complexity, but worse in tests. This helps to indicate the importance of the dispersal properties of different DPDs since DDR1 is the least dispersive among all pruning DPDs. It gets more evident when the PA is operated at a 4.4-dB back-off output power as described below.

3.3 Scenario 2: output power at 4.4-dB back-off

The PA can be driven harder for a better power efficiency, but producing more nonlinear characteristics. Also, the increase of dynamic cross terms is included as the interaction between the PA nonlinearities and I/Q imbalance is

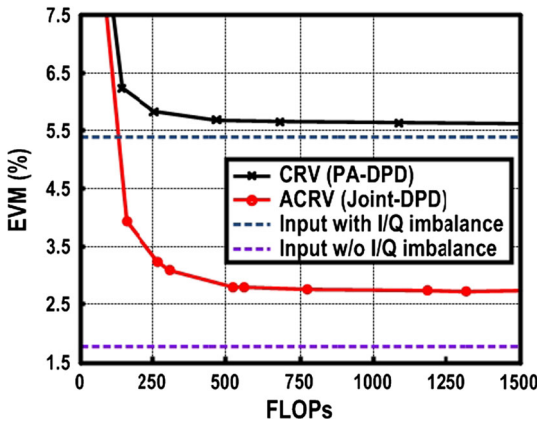

Fig. 9 Scenario 2: Output power at 4.4-dB back-off from the saturation power. Comparison between CRV and ACRV via EVM versus FLOPs

amplified. It leads to performance degradation to all DPDs in both simulations and measurements. Comparisons respect to PA-/joint-DPD and inter-joint-DPD are given in Figs. 9 and 10, respectively. As described previously, the best performance parameters causing complexity <1000 FLOPs are selected for forward validation. For ACRV, the selected configuration is (7, 3, 5, 1) with 809 FLOPs.

The features of the input signal are the same as the scenario 1. The constellation diagrams in Fig. 11 show that

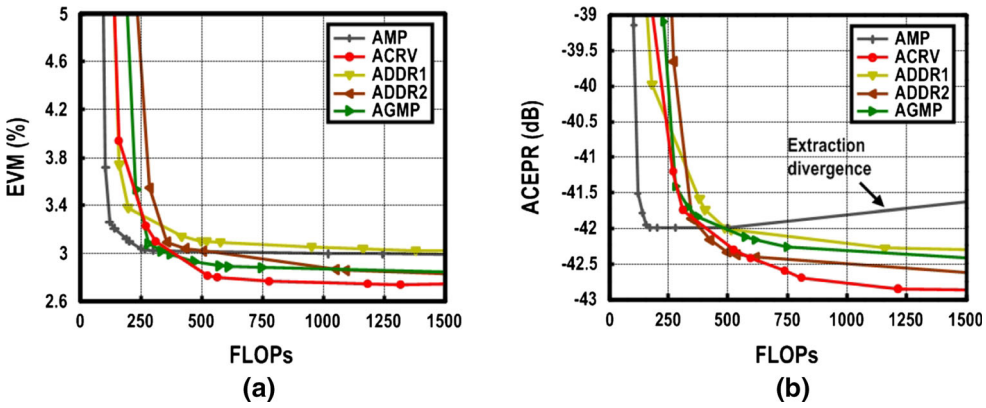

Fig. 10 Scenario 2: Output power at 4.4-dB back-off from the saturation power. ADDR1 and ADDR2 stand for asymmetrical first- and second-order Volterra DDR joint DPDs, respectively. **a** EVM versus FLOPs. **b** ACEPR versus FLOPs

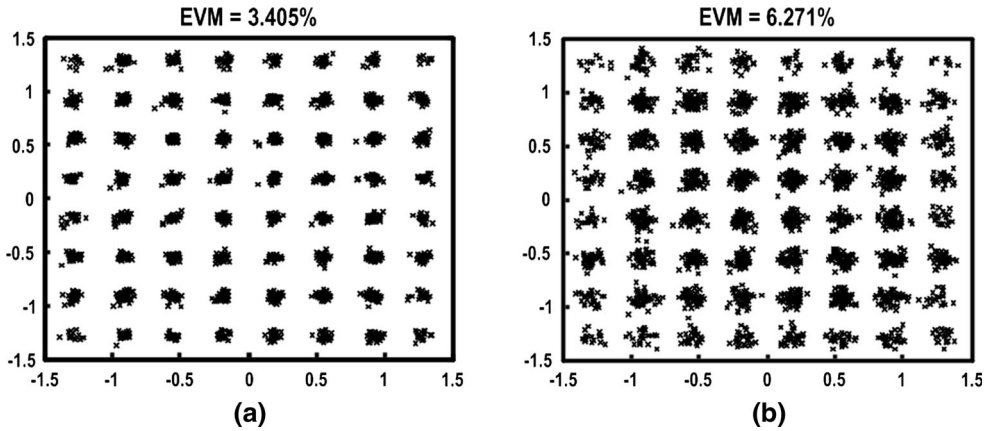

Fig. 11 Scenario 2: Output power at 4.4-dB back-off from the saturation power. Measured constellation diagrams: **a** system output with ACRV joint-DPD, and **b** with CRV PA-DPD

the proposed ACRV can improve the system EVM significantly from 22.1 to 3.4 %, while the CRV is limited with EVM of 6.27 %. The AM/AM and AM/PM plots for the system output without and with proposed ACRV joint-DPD are presented in Fig. 12(a, b), respectively. The (left, right) ACPR of system output is improved from (−19.9 dBc, −19.6 dBc) to (−37.3 dBc, −37.9 dBc). Spectra of the compensated system output with different DPDs are presented in Fig. 12(c).

The practicability of this scenario is of concern. In Table 3, the key parameters for five different DPDs are listed. From Table 3, AMP, AGMP, ADDR1 and ADDR2 show similar performance in simulations, but vary significantly in tests. Only the measured ACPR of ADDR2 is improved similarly to of ACRV. Compare to the performance of measured EVM, AMP, AGMP, ADDR1 and ADDR2 cannot be suppressed even compare to PA-DPD of CRV alone. This strongly indicated the basis construction affects the jointly mitigation performance as they cannot address the interaction between I/Q imbalance and the nonlinear memory effect. AGMP is better than AMP in simulations, at the expense of $>3\times$ of complexity. Yet, the increase of the number of coefficients affects the accuracy of the LS extraction, showing a similar EVM but worse ACPR. The proposed ACRV shows consistent results in both simulations and measurements under diagonal dispersal properties, while outperforming the others obviously in terms of EVM and ACPR reduction in the range FLOPs <1000. For the complexity-efficiency issue, 595-FLOPs ACRV is chosen to compare to others DPD, a similar performance is achieved.

4 Discussion

For the above two scenarios, all results from measurements are degraded when comparing with those from simulations. This is due to various kinds of systematic noise and imperfection. The crucial one is the quantization noise from both the VSG and DSO, especially because the DUT is a medium-power PA.

Both the orders of nonlinearities and basis construction play a key role in joint-DPD. From Tables 2 and 3, at least 11th-order nonlinearities are deployed for each DPD. The diagonal dispersal AMP with *P*th-order dynamics consistently beating ADDR1 shows that the dynamic order

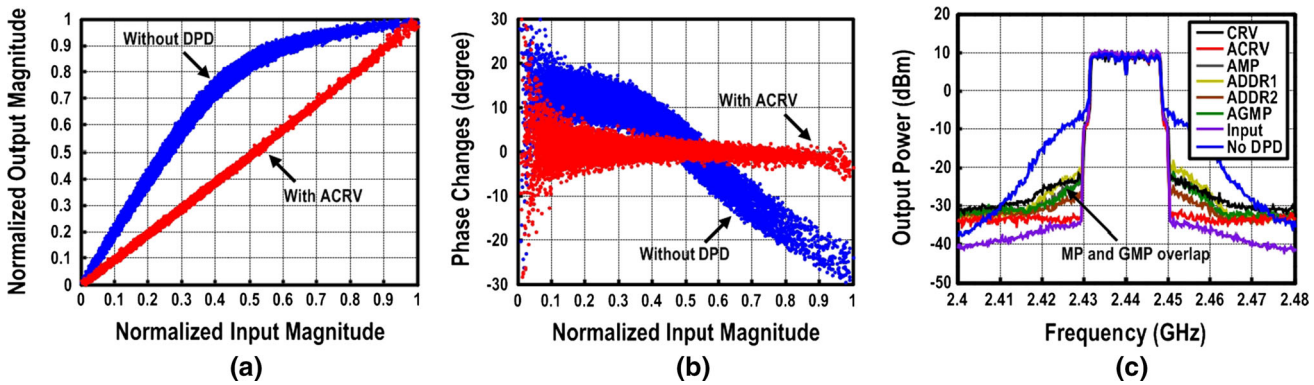

Fig. 12 Scenario 2: Output power at 3.4-dB back-off from the saturation power. **a** AM/AM and **b** AM/PM plots for the system output without DPD, and with proposed ACRV joint-DPD. **c** Spectra plots of the system input, output without DPD and output with different kinds of joint-DPDs

Table 3 Selected parameters of each DPD for performance validation

Model	Parameters	FLOPs	$ACEPR_{sim}$	EVM_{sim}	EVM_{meas}	$ACPR_{sim}$	$ACPR_{meas}$
ACRV	(7,3,5,1)	809	−42.69	2.768	3.405	(−38.12, −38.15)	(−37.3, −37.9)
ACRV (2)	(7,2,5,1)	595	−42.52	2.831	3.520	(−38.06, −38.10)	(−37.0, −37.5)
AMP	(11,1,7,2)	203	−42.00	3.186	5.206	(−37.54, −37.93)	(−33.4, −34.0)
ADDR1	(11,3,7,1)	519	−42.02	3.099	6.367	(−37.58, −37.50)	(−33.2, −32.2)
ADDR2	(11, 1,11, 1)	625	−42.41	3.010	4.417	(−37.80, −38.15)	(−35.2, −34.8)
AGMP	(11,2,2,7,1,1)	741	−42.26	2.880	5.221	(−37.72, −37.76)	(−33.6, −32.6)

Corresponding simulated and experimental calibrating performance for Scenario 2

involved in the basis construction contributes to the joint-DPD performance. Besides, by comparing AMP and AGMP, it can be observed that the diversity of the cross terms with the same dynamic order may not help the performance much, as AGMP cannot address to the interaction between I/Q imbalance and nonlinear memory effect. Also, serious complexity is added. As a result, the proposed ACRV structure is capable to outperform others, in which its basis construction containing large dispersive orders of nonlinearities, cross terms and dynamics with unit memory depths can make the joint-DPD better and more efficient in complexity.

5 Conclusions

An asymmetrical complexity-reduced Volterra series (ACRV) model is proposed as the joint-DPD, which is derived from the analysis of the interaction between I/Q imbalance and PA nonlinearities. Dispersal properties of different DPDs have been introduced to describe the difference between basis constructions of pruning schemes. Based on our OFDM-signal study an asymmetrical structure is developed by abandoning insignificant nonlinear terms to reduce the computational complexity. The running complexity in terms of FLOPs is analyzed. LS estimation is then deployed for extracting the kernels of proposed ACRV. The Qhull algorithm helps to find the best performance parameters of the proposed ACRV with FLOPs <1000. From the measurement results given in Tables 2 and 3, the relationship $P \geq P_i, M \geq M_i$ was applicable to all DPDs, which indicates that the proposed asymmetrical structure also relaxes the computational complexity. Benefiting from the diagonal dispersal properties of basis construction containing high orders of nonlinearities and dynamics with large memory depths, the proposed ACRV structure achieves the best simulation-to-validation practicability, and outperforms other competitive DPDs in terms of EVM and ACPR reduction, especially under the interaction between I/Q imbalance with severe non-idealities.

Acknowledgments This work is funded by the Macau Science and Technology Development Fund (FDCT) – SKL Fund and the University of Macau - MYRG2015-00040-FST.

Appendix

The formulas for calculating the complexity of extended joint-DPDs of AMP, ADDR with first and second order dynamic and AGMP are listed as follows
AMP:

$$C_{\text{AMP,basis}}(P,M,P_i,M_i) = 3 + (\max(P,P_i) - 1)$$

$$f_{\text{AMP}}(P,M,P_i,M_i) = \left(\frac{P+1}{2}\right)(M+1) + \left(\frac{P_i+1}{2}\right)(M_i+1)$$

ADDR with first order dynamic:

$$\begin{aligned} C_{\text{ADDR1,basis}}(P,M,P_i,M_i) &= 9 \\ &+ \max[(M+1)(P-1),(M_i+1)(P_i-1)] \\ &+ 6\max\left[M\left(\frac{P-3}{2}\right), M_i\left(\frac{P_i-3}{2}\right)\right] \end{aligned}$$

$$f_{\text{ADDR1}}(P,M,P_i,M_i) = \frac{P+1}{2}(1+M) + \frac{P-1}{2}M + \frac{P_i+1}{2}(1+M_i) + \frac{P_i-1}{2}M_i$$

ADDR with second order dynamic:

$$\begin{aligned} C_{\text{ADDR2,basis}}(P,M,P_i,M_i) &= 15 + 6\max(M,M_i) \\ &+ \max[(M+1)(P-1),(M_i+1)(P_i-1)] \\ &+ 6\max\left[M\left(\frac{P-3}{2}\right), M_i\left(\frac{P_i-3}{2}\right)\right] \\ &+ 6\max\left[\left(\frac{P-3}{2}\right)\left(M^2 + \frac{M(M+1)}{2}\right), \left(\frac{P_i-3}{2}\right)\left(M_i^2 + \frac{M_i(M_i+1)}{2}\right)\right] \\ &+ 6\max\left[\left(\frac{P-5}{2}\right)\frac{M(M+1)}{2}, \left(\frac{P_i-5}{2}\right)\frac{M_i(M_i+1)}{2}\right] \end{aligned}$$

$$\begin{aligned} f_{\text{ADDR2}}(P,M,P_i,M_i) &= \frac{P+1}{2}(1+M) \\ &+ \frac{P-1}{2}\left(M + \frac{M(M+1)}{2} + M^2\right) + \frac{P-3}{2}\frac{M(M+1)}{2} \\ &+ \frac{P_i+1}{2}(1+M_i) + \frac{P_i-1}{2}\left(M_i + \frac{M_i(M_i+1)}{2} + M_i^2\right) \\ &+ \frac{P_i-3}{2}\frac{M_i(M_i+1)}{2} \end{aligned}$$

AGMP with only odd-order nonlinearities and causal terms:

$$\begin{aligned} C_{\text{AGMP,basis}}(P,M,K,P_i,M_i,K_i) &= 3 + [\max(P,P_i) - 1] \\ &+ \max[(P-3)K,(P_i-3)K_i] \\ &+ \left[(P-3)\frac{M(M+1)}{2}, (P_i-3)\frac{M_i(M_i+1)}{2}\right] \end{aligned}$$

$$\begin{aligned} f_{\text{AGMP}}(P,M,K,P_i,M_i,K_i) &= (M+1)\left[\frac{P+1}{2} + \frac{(P-1)}{2}K\right] \\ &+ \frac{(P-1)}{2}\frac{M(M+1)}{2} + (M_i+1)\left[\frac{P_i+1}{2} + \frac{(P_i-1)}{2}K_i\right] \\ &+ \frac{(P_i-1)}{2}\frac{M_i(M_i+1)}{2} \end{aligned}$$

Note that for AGMP, the parameters of (14) are represented by (P,M,K,P_i,M_i,K_i) where K and K_i are the leading and lagging depth [12] for the signal and its image, respectively.

References

1. Bingham, J. (1990). Multicarrier modulation for data transmission: An idea whose time has come. *IEEE Communications Magazine, 5*, 5–14.
2. Come, B., Ness, R., Donnay, S., Van der Perre, L., Eberle, W., Wambacq, P., Engels, M., Bolsens, I. (2000) Impact of front-end nonidealities on bit error rate performance of WLAN-OFDM transceivers. In *Proceedings on RAWCON* (pp. 91–94).
3. Ding, L., Ma, Z., Morgan, D. R., Zierdt, M., & Zhou, G. T. (2008). Compensation of frequency-dependent gain/phase imbalance in predistortion linearization systems. *IEEE Transactions on Circuits Systems I: Regular Papers, 55*(1), 390–397.
4. Schreurs, D., O'Borma, M., Goacher, A. A., & Gadringer, M. (2008). *RF power amplifier behavioral modeling*. Cambridge, UK: Cambridge University Press.
5. Fettweis, G., Lohning, M., Petrovic, D., Windisch, M., Zillmann, P., Rave, W. (2005). Dirty RF: A new paradigm, *IEEE 16th International Symposium on Personal, Indoor and Mobile Radio Communication* (vol 4, pp. 2347–2355).
6. Fager, C., Pedro, J. C., de Carvalho, N. B., Zirath, H., Fortes, F., & Rosario, M. J. (2004). A comprehensive analysis of IMD behavior in RF CMOS power amplifiers. *IEEE Journal of Solid-State Circuits, 39*(1), 24–34.
7. Chen, S. (2011). An efficient predistorter design for compensating nonlinear memory high power amplifiers. *IEEE Transactions on Broadcasting, 57*(4), 856–865.
8. Jiang, H., & Wilford, P. A. (2010). Digital predistortion for power amplifiers using separable functions. *IEEE Transactions on Signal Processing, 58*(8), 4121–4130.
9. Crespo-Cadenas, C., Reina-Tosina, J., Madero-Ayora, M. J., & Munoz-Cruzado, J. (2010). A new approach to pruning volterra models for power amplifiers. *IEEE Transactions on Signal Process, 58*(4), 2113–2120.
10. Mirri, D., et al. (2002). A modified Volterra series approach for nonlinear dynamic systems modeling. *IEEE Transactions on*

Circuits Systems I: Fundamental Theory on Applications, 49(8), 1118–1128.
11. Kim, J., & Konstantinou, K. (2001). Digital predistortion of wideband signals based on power amplifier model with memory. *IET Electronics Letters, 37*(23), 1417–1418.
12. Zhu, A., Draxler, P. J., Yan, J. J., Brazil, T. J., Kinbal, D. F., & Asbeck, P. M. (2008). Open-loop digital predistorter for RF power amplifiers using dynamic deviation reduction-based Volterra series. *IEEE Transactions on Microwave Theory and Techniques, 56*(7), 1524–1534.
13. Morgan, D. R., Ma, Z., Kim, J., Zierdt, M. G., & Pastalan, J. (2006). A generalized memory polynomial model for digital predistortion of RF power amplifiers. *IEEE Transactions on Signal Processing, 54*(10), 3852–3860.
14. Mkadem, F., Fares, M. C., Boumaiza, S., & Wood, J. (2014). Complexity- reduced Volterra series model for power amplifier digital predistortion. *Analog Integrated Circuits and Signal Processing, 79*(2), 331–343.
15. Li, Y., Cheang, C.-F., Mak, P.-I., & Martins, R. P. (2016). The dispersal analysis on basis construction of digital predistortion techniques for power amplifier. *Analog Integrated Circuits and Signal Processing, 86*, 77–86.
16. Cao, H., Tehrani, A. S., Fager, C., Eriksson, T., & Zirath, H. (2009). I/Q imbalance compensation using a nonlinear modeling approach. *IEEE Transactions on Microwave Theory and Techniques, 57*(3), 513–518.
17. Kim, Y.-D., Jeong, E.-R., & Lee, Y. H. (2007). Adaptive compensation for power amplifier nonlinearity in the presence of quadrature modulation/demodulation errors. *IEEE Transactions on Signal Processing, 55*(9), 4717–4721.
18. Anttila, L., Händel, P., & Valkama, M. (2010). Joint mitigation of power amplifier and I/Q modulator impairments in broadband direct-conversion transmitters. *IEEE Transactions on Microwave Theory and Techniques, 58*(4), 730–739.
19. Schubert, B., Gokceoglu, A., Anttila, L., Valkama, M. (2013). Augmented Volterra predistortion for the joint mitigation of power amplifier and I/Q modulator impairments in wideband flexible radio. In *Global conference on signal and information processing* (*GlobalISIP*) (pp. 1162–1165). IEEE.
20. Gregorio, F., Cousseau, J., Werner, S., Riihonen, T., & Wichman, R. (2011). Power amplifier linearization technique with IQ imbalance and crosstalk compensation for broadband MIMO-OFDM transmitters. *EURASIP Journal on Advances in Signal Processing, 2011*(1), 1–15.
21. Tehrani, A. S., Cao, H., Afsardoost, S., Eriksson, T., Isaksson, M., & Fager, C. (2010). A comparative analysis of the complexity/accuracy tradeoff in power amplifier behavioral models. *IEEE Transactions on Microwave Theory and Techniques, 58*(6), 1510–1520.
22. Cunha, T. R., Pedro, J. C., Lima, E. G. (2008). Low-pass equivalent feedback topology for power amplifier modeling. In *IEEE MTT-S international microwave symposium on digest* (pp. 1445–1448).
23. Mazière, C., Soury, A., Ngoya, E., Nébus, J. (2005). A system level model of solid state amplifiers with memory based on a nonlinear feedback loop principle. In *IEEE International European Microwave Conference*, Paris (vol. 1, pp. 853–856).
24. Xiao, Y., He, G., Ma, J. (2009). A novel method for estimation and compensation of transmitter I/Q imbalance. In *international SoC design conference* (pp. 261–265).
25. Schetzen, M. (2006). *The Volterra and Wiener Theories of Nonlinear Systems*. Malabar, FL: Krieger.
26. Ljung, L. (1999). *System Identification: Theory for the User* (2nd ed.). Englewood Cliffs, NJ: Prentice-Hall.

Yue Li received the B.Sc. Degree in Electrical and Electronics Engineering from the University of Macau, Macao SAR, China, in 2012, and received his M.Sc. Degree in 2014 at the UM State-Key Laboratory of Analog and Mixed-Signal VLSI and Faculty of Science and Technology (ECE) from University of Macau, Macao, China.

Chak-Fong Cheang received his B.Sc. and his M.Sc. Degree in Department of Engineering Science from National Cheng Kung University (NCKU), Tainan, Taiwan, in 2008, 2010. He is currently working toward the Ph.D. Degree at the UM State-Key Laboratory of Analog and Mixed-Signal VLSI and Faculty of Science and Technology (ECE) from University of Macau, Macao, China. His research interests are digital predistortion and digital mitigation on RF impairment and field-programmable gate-array (FPGA)-based embedded signal processing.

Pui-In Mak (S'00-M'08-SM'11) received the Ph.D. Degree from University of Macau (UM), Macao SAR, China, in 2006. He is currently Associate Professor at UM, and Coordinator of the Wireless & Biomedical Research Lines of the *State-Key Laboratory of Analog and Mixed-Signal VLSI*. His research interests are on analog and RF circuits and systems for wireless, biomedical and physical chemistry applications. His involvements with IEEE are: Distinguished Lecturer ('14–'15) and Member of Board-of-Governors ('09–'11) of IEEE Circuits and Systems Society (CASS); Editorial Board Member of IEEE Press ('14–'16); Senior Editor of IEEE Journal on Emerging and Selected Topics in Circuits and Systems ('14–'15); Associate Editor of IEEE Transactions on Circuits and Systems Part I (TCAS-I) ('10–'11, 14′–); Associate Editor of IEEE Transactions on Circuits and Systems Part II (TCAS-II) ('10–'13), and Guest Editor of IEEE RFIC Virtual Journal ('14). Professor Mak received IEEE DAC/ISSCC Student Paper Award'05; IEEE CASS Outstanding Young Author Award'10; National Scientific and Technological Progress Award'11; Best Associate Editor for TCAS-II'12–'13. In 2005, he was decorated with the *Honorary Title of Value* for scientific merits by the Macau Government. He is currently the Technical Program Committee (TPC) Member of ISSCC, ESSCIRC and A-SSCC. He was the TPC Vice-Chair of ASP-DAC ('16).

Rui P. Martins (M'88-SM'99-F'08), born in April 30, 1957, received the Bachelor (5-years), the Masters, and the Ph.D. Degrees, as well as the *Habilitation* for Full-Professor in electrical engineering and computers from the Department of Electrical and Computer Engineering, Instituto Superior Técnico (IST), TU of Lisbon, Portugal, in 1980, 1985, 1992 and 2001, respectively. He has been with the Department of Electrical and Computer Engineering (DECE)/IST, TU of Lisbon, since October 1980. Since 1992, he is also with the Department of Electrical and Computer Engineering, Faculty of Science and Technology (FST), University of Macau (UM), Macao, China, where he is currently a Chair-Professor since August 2013. In FST he was the Dean of the Faculty from 1994 to 1997 and he has been Vice-Rector of the University of Macau since 1997, being Vice-Rector (Research) since 2008. He created in 2003 the *Analog and Mixed-Signal VLSI Research Laboratory* of University of Macau, elevated in January 2011 to State Key Laboratory of China (the 1st in Engineering in Macao), being its Founding Director. Professor Rui Martins is an *IEEE Fellow*, was the Founding Chairman of IEEE Macau Section (2003–2005), and IEEE Macau Joint-Chapter on CAS/COM (2005–2008) [2009 *World Chapter of the Year* of the *IEEECAS Society*]. He was Vice-President for Region 10 of *IEEE CASS* (2009–2011), Vice-President (World) Regional Activities and Membership of *IEEE CASS* (2012–2013), and Associate Editor of *IEEE T-CAS II: Express Briefs* (2010–2013), nominated *Best Associate Editor* for 2012–2013. Plus, he was a member of the IEEE CASS Fellow Evaluation Committee (Classes of 2013 and 2014). He was the recipient of 2 government decorations: the Medal of Professional Merit from Macao Government (Portuguese Administration) in 1999, and the Honorary Title of Value from Macao SAR Government (Chinese Administration) in 2001. In July 2010 was elected, unanimously, as Corresponding Member of the Portuguese Academy of Sciences (in Lisbon), being the only Portuguese. Academician living in Asia.